Available online at www.sciencedirect.com

SciVerse ScienceDirect

Acta Materialia 61 (2013) 3687–3694

Acta MATERIALIA

www.elsevier.com/locate/actamat

Giant electrostrains accompanying the evolution of a relaxor behavior in $Bi(Mg,Ti)O_3$–$PbZrO_3$–$PbTiO_3$ ferroelectric ceramics

Jian Fu, Ruzhong Zuo *

Institute of Electro Ceramics & Devices, School of Materials Science and Engineering, Hefei University of Technology, Hefei 230009, People's Republic of China

Received 3 January 2013; received in revised form 20 February 2013; accepted 28 February 2013
Available online 20 March 2013

Abstract

Extremely enhanced electrostrains (up to 0.39%) were surprisingly observed in $(0.67 - x)Bi(Mg_{0.5}Ti_{0.5})O_3$–$xPbZrO_3$–$0.33PbTiO_3$ (BMT–*x*PZ–PT) ternary solid solutions, possibly resulting in BMT–*x*PZ–PT ceramics having great potential for large-displacement actuator applications. The generation of giant strains was found to be closely associated with the evolution of a weak relaxor behavior from diffuse-type BMT–PT binary ferroelectrics, during which the domain switching is actively facilitated owing to a change in the dynamics of the polar nanoregions from a static state to a dynamic state. It can be also attributed to a ferroelectric nature of the evolved relaxors in PZ substituted BMT–PT ceramics instead of a dipole glass freezing state. These judgements were reasonably supported by a couple of measurements, including strains vs. electric field, Raman scattering, dielectric spectroscopy and the time- and electric-field-dependent polarization. The present study can provide a general approach towards an appropriate compositional design for large electrostrains in BMT-based and related systems.

Keywords: Ferroelectric; Relaxor; Dielectric; Domain switching; Strain

1. Introduction

Increasing attention has recently been focused on developing materials capable of large strains for actuator applications [1–4]. These materials were usually based on relaxors, antiferroelectrics and ferroelectrics. For typical relaxors such as $Pb(Mg_{1/3}Nb_{2/3})O_3$ (PMN), the electric-field-induced strain is usually dominated by an electrostrictive effect and is basically proportional to the square of the polarization or to the applied electric field. However, this kind of strain is generally weak and can be nearly neglected in ferroelectrics with a strong piezoelectric response. For anti-ferroelectrics, the electrostrain generally results from a large volume expansion during an anti-ferroelectric–ferroelectric phase transformation [5,6].

The electric-field-induced butterfly-like hysteretic strain loops in ferroelectrics are basically due to both the intrinsic and extrinsic contributions. The intrinsic contribution is mainly referred to the (converse) piezoelectric effect, i.e. the variation of the lattice distortion, which is proportional to the applied electric field. A common approach to enhancing the intrinsic contribution (lattice strain) used to be the adjustment of the chemical compositions within a coexistence zone of two ferroelectric phases. In this case, a considerable electrostrain is usually associated with field-induced inter-ferroelectric phase transformation [1–3], accompanied by a change in the lattice distortion between different phases [7–16]. The intrinsic contribution becomes more pronounced in Pb-based relaxor ferroelectric crystals, accounting for more than 95% of the total piezoelectric response for compositions lying at the rhombohedral-rich side of the rhombohedral–monoclinic phase boundary [17]. By comparison, the extrinsic contribution to strains is mainly from the domain switching, during which the

* Corresponding author. Tel./fax: +86 551 62905285.
E-mail address: piezolab@hfut.edu.cn (R. Zuo).

1359-6454/$36.00
http://dx.doi.org/10.1016/j.actamat.2013.02.055

ferroelectric materials change their spontaneously polarized states along the applied electric field direction. The magnitude of the strain generated during domain switching depends on the type of the domains being switched and the extent of the lattice anisotropy. For this reason, large electrostrains as high as 1 and 6.5% were expected in tetragonal $BaTiO_3$ and $PbTiO_3$ (PT) crystals, respectively, owing to their different c/a ratios [2]. However, it is not easy achieving such high strain values in polycrystalline ceramics owing to the clamping effect caused by neighboring domains and grains with different orientations [18]. Therefore, commercial Pb-based perovskite ferroelectric ceramics usually have a relatively low electrostrain (<0.2%), regardless of their excellent piezoelectric responses in the vicinity of a morphotropic phase boundary (MPB) [1].

$Bi(Mg_{0.5}Ti_{0.5})O_3$–$PbTiO_3$ (BMT–PT) ferroelectric materials have recently attracted much attention owing to their high Curie temperatures, moderate piezoelectric and electromechanical responses, and potential usages for zero thermal expansion materials [19–25]. Unfortunately, their ferroelectricity and electrostrains are inferior to those of typical $Pb(Zr,Ti)O_3$ (PZT)-based ferroelectric ceramics. It was reported that rhombohedral BMT–PT compositions exhibit an obvious diffuse phase transition without any frequency dispersion, although BMT–PT belongs to the B-site complex perovskite materials. The enhanced ferroelectricity was observed in the quenched $Bi(Zn_{1/2}Ti_{1/2})O_3$ (BZT) substituted BMT–PT ceramics, where a relaxor behavior was formed by changing thermal quenching conditions [25]. In this study, the addition of PZ was expected to induce a weak relaxor ferroelectric behavior with a nonergodic relaxor state (quasi-ferroelectric state), leading to a change in the dynamics of polar nanoregions from a static state to a dynamic state. This change was found to be accompanied by a significant enhancement of the electrostrain. As a result, we successfully prepared giant-strain BMT–PZ–PT ternary solid solution ceramics with a great potential for large-displacement actuator materials. The mechanism of generating large electrostrains by incorporating unipolar/bipolar electric-field-induced strain loops, dielectric constant vs. temperature curves, polarization current density curves and Raman spectra is discussed.

2. Experimental

The ceramic samples of BMT–xPZ–PT ($x = 0$–0.67) were prepared by a conventional solid state reaction method using high-purity raw materials. The mixed powders were calcined at 830 °C for 4 h and then ball-milled again for 24 h. Sintering was carried out in air in the temperature range of 1000–1200 °C for 2 h. The crystal structure of the as-sintered ceramics was examined by a powder X-ray diffractometer (D/MAX2500VL/PC, Rigaku, Japan) using Cu $K_{\alpha 1}$ radiation. For the electrical measurements, silver paste was painted on both sides of the samples and fired at 550 °C for 30 min. The dielectric properties were measured using an LCR meter (E4980A, Agilent, Santa Clara, CA) from room temperature to 600 °C. The polarization vs. electric field (P–E) hysteresis loops and strain vs. electric field curves were measured by using a ferroelectric test system (Precision LC, Radiant Technologies Inc., Albuquerque, NM) connected with a laser interferometric vibrometer (SP-S 120, SIOS Meβtechnik GmbH, Germany) at a fixed frequency of 1 Hz. Raman spectra were collected in a backscattering geometry using 514.5 nm excitation line from LabRAM HR800 spectrometer (JY, Longjumeau Cedex, France) at room temperature.

3. Results

3.1. Structure analysis

Fig. 1a shows a schematic phase diagram of the BMT–PZ–PT ternary system based on the work of Jaffe et al. [26] and Randall et al. [19], in which the blue dashed line stands for the approximate position of the MPB for the BMT–PZ–PT ternary system. The selected compositions were plotted as red dots and located at the upper side of

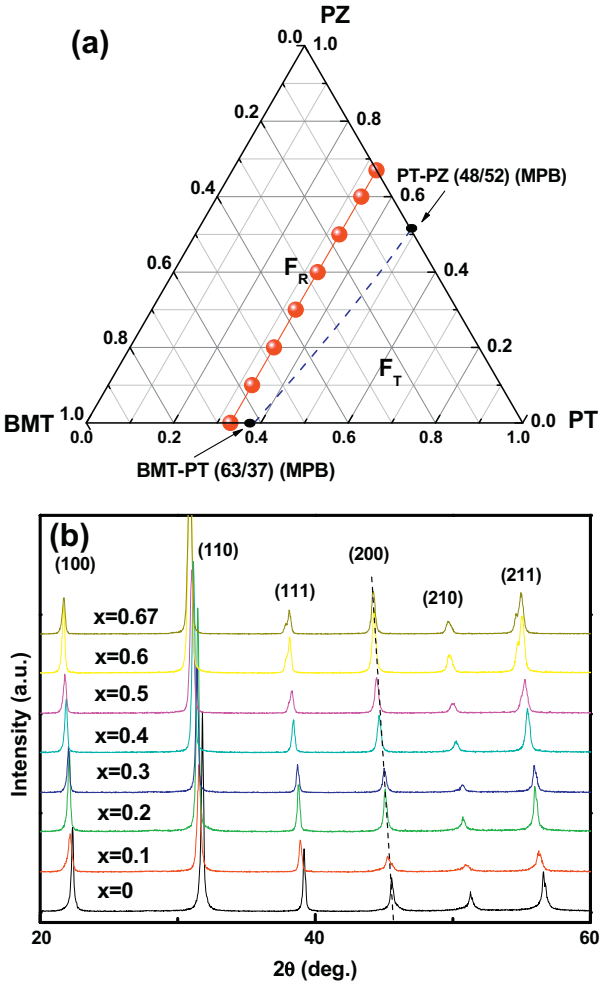

Fig. 1. (a) Phase diagram of BMT–PZ–PT ternary system, and (b) X-ray diffraction patterns of (0.67 – x)BMT–xPZ–0.33PT compositions as indicated.

the MPB line. It is thus expected that all studied compositions should exhibit a rhombohedral perovskite structure, as confirmed by room-temperature X-ray diffraction analysis in Fig. 1b. Nevertheless, the diffraction peaks shift to lower diffraction angles with increasing the PZ content, indicating that there is a slight lattice expansion. This is probably due to relatively large ionic radii of Pb^{2+} and Zr^{4+} compared to those of Bi^{3+} and $(Mg^{2+}_{0.5}Ti^{4+}_{0.5})$ at the A- and B-sites ($CN = 12$, $R_{Pb} = 1.49$ Å, $R_{Bi} = 1.45$ Å; $CN = 6$, $R_{Zr} = 0.72$ Å, $R_{Mg} = 0.72$ Å, $R_{Ti} = 0.605$ Å), respectively [27].

3.2. Giant electrostrain of $(0.67 - x)$BMT–xPZ–0.33PT ceramics

Fig. 2a and b shows the strains as a function of bipolar and unipolar electric fields at room temperature for $(0.67 - x)$BMT–xPZ–0.33PT (BMT–xPZ–PT) ceramics, respectively. As can be seen from Fig. 2a, all samples show typical electric-field-induced butterfly strain loops, meaning that these compositions exhibit obvious ferroelectric behavior. However, only a small poling strain can be observed for 0.67BMT–0.33PT ceramics. That is to say, both positive (S_{pos}) and negative (S_{neg}) strains are low. This result further confirmed that rhombohedral BMT–PT compositions only possess relatively poor ferroelectric and piezoelectric properties [19]. A drastic increase of both S_{pos} and S_{neg} could be found after the addition of PZ. The maximum S_{pos} and S_{neg} values were found to appear in the compositions with $x = 0.2$ and $x = 0.4$, respectively. S_{neg} is denoted by the difference between the minimum strain and the strain at zero electric field during bipolar cycles, and represents the amount of irreversible non-180° domains. It is generally considered as the remanent strain (S_r) after removal of the electric field, in which no piezoelectric strain (S_{piezo}) is present owing to the absence of external electric field [28]. As a result, the increase of the S_{neg} value indicates the increase of the contribution from non-180° irreversible domain switching. S_{pos} can be considered as an additional strain of the post-poled samples as the electric field is applied. This process would involve domain switching in addition to the piezoelectric effect. Therefore, S_{pos} should be the sum of the piezoelectric strain and the extra strain (S_{switch}) from the domain switching. The strain under unipolar cycles (S_E) should be equal to the poling strain minus remanent strain (S_{pol}–S_r) under a bipolar cycle. That is to say, S_E is just equal to the S_{pos} under bipolar cycles. Moreover, it is indicated from Fig. 2a and b that all compositions exhibit nonlinear and hysteretic strain loops except for the samples $x = 0.6$ and 0.67. The nonlinearity of the strains becomes most pronounced in the samples with $x = 0.1$, 0.2 and 0.3. These three compositions also exhibit relatively large electrostrains and the largest value (S_E~0.39%) can be obtained in the $x = 0.2$ sample. Although the $x = 0.4$ composition exhibits a large S_{neg} (see Fig. 2a), its S_E value is relatively small. This might be resulting from a small S_{switch} contribution in this composition. Similarly, a nearly linear and small-hysteresis unipolar strain curve was obtained in the $x = 0.4$ sample. The strains such as S_{pos}, S_{neg}, S_E, S_{switch} and S_{pol} were extracted and plotted as a function of the PZ content in Fig. 2c. It was surprisingly observed that the generated strains in BMT–xPZ–PT ternary systems are even higher than those in the soft ferroelectric PZT ceramics and comparable to those in Pb-based antiferro-

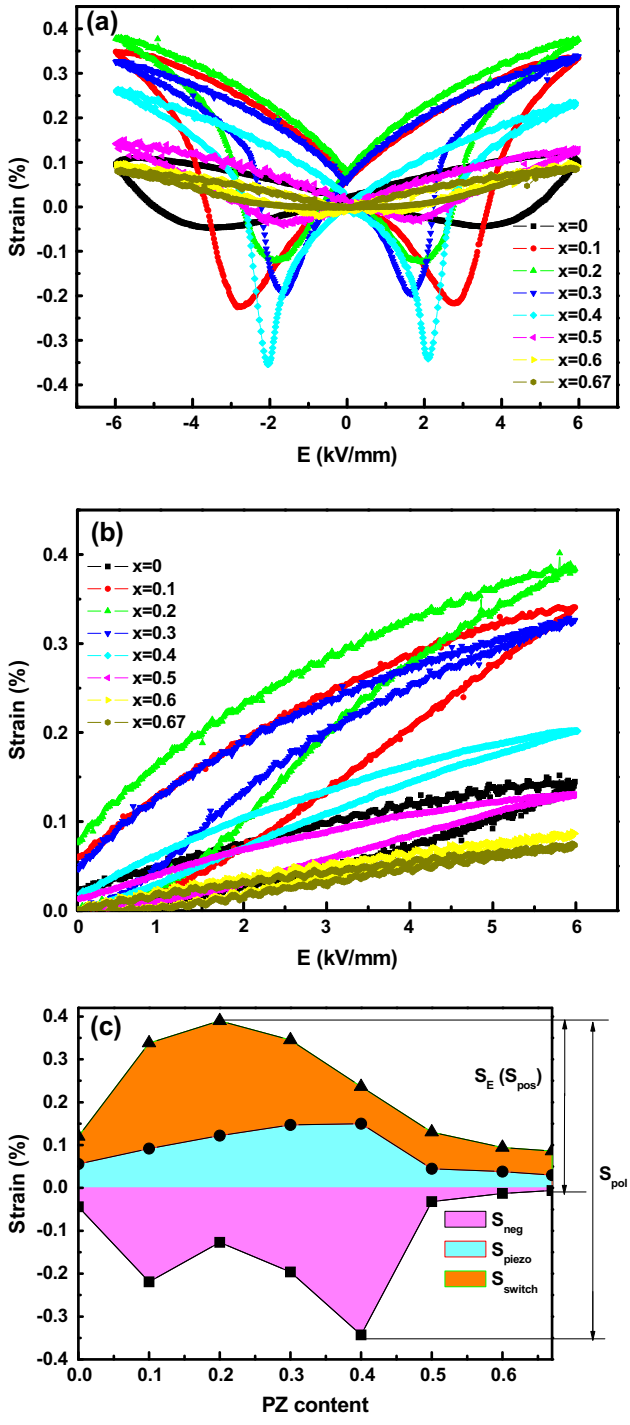

Fig. 2. Strains as a function of (a) bipolar and (b) unipolar electric fields, and (c) the extracted S_E (S_{pos}), S_{neg}, S_E, S_{pol}, S_{switch} and S_{piezo} values as a function of the PZ content for BMT–xPZ–PT ferroelectric ceramics.

electrics. Most interestingly, it can be clearly seen that the giant strain in the $x = 0.2$ sample was dominantly ascribed to the enhanced domain switching contribution.

3.3. Dielectric spectroscopy

Fig. 3 shows the temperature and frequency dependencies of the dielectric constant of the BMT–xPZ–PT ceramics. It can be obviously seen that the dielectric behavior of the BMT–xPZ–PT ceramics changes drastically with the addition of PZ. For BMT–PT binary composition ($x = 0$), a typical diffuse phase transition (DPT) behavior was found but no frequency dispersion was observed. This is usually considered as an intermediate state between normal ferroelectrics and relaxor ferroelectrics [29]. By comparison, the 0.67PZ–0.33PT binary composition exhibits an evident normal ferroelectric behavior. With increasing the PZ concentration, the dielectric peaks at the dielectric maxima become more diffuse and more frequency-dependent. This phenomenon seemed to be observed in the PZ doped BZT–PT binary system [30]. The above change means that there is a diffuse–relaxor–normal ferroelectric transformation in the studied compositions from the BMT-rich side to the PZ-rich side.

The size and dynamics of the polar nanoregions (PNRs) were believed to play an important role in the relaxor behavior [31]. At high temperatures, the size of the PNRs is small enough and weakly correlated with each other, such that they can exhibit a dynamic behavior, leading to the frequency dispersion of the dielectric constant. With decreasing the temperature, the average size of PNRs increases and their dynamics slows down. As a result, a nonergodic relaxor state (or dipole glass) [32,33] or ferroelectric state [34–36] can appear at low temperatures. As a ferroelectric state is induced, there should be a critical temperature T_{nr} (T_{rn}) that corresponds to the spontaneous normal–relaxor (heating) or relaxor–normal (cooling) transformation. As shown in Fig. 3, the compositions should exhibit a nonergodic relaxor state (or dipole glass) at room temperature in the range of $x = 0.10$–0.30, but ferroelectric order state as $x = 0.4$–0.5, because a spontaneous normal–relaxor ferroelectric transformation can be obviously observed near the $x = 0.5$ composition. Moreover, the frequency-independent DPT behavior in the $x = 0$ sample could be considered as a result of different PNR sizes corresponding to different relaxation frequencies beyond the scope of the experimental frequencies [29].

It is of interest to note that BMT belongs to a typical B-site complex perovskite material similar to canonical relaxors, such as PMN. Therefore, the chemical disorder of B-site Mg^{2+} and Ti^{4+} ions with different charges might also generate random local electric fields, which could be coupled to the local polarization owing to local charge imbalances. Thus, pure BMT seems possible to exhibit a relaxor behavior [37]. However, it is rather difficult to synthesize it. By comparison, an additional random local strain field could exist in BMT–PT solid solutions owing to different sizes of A- and B-site ions ($CN = 12$, $R_{Pb} = 1.49$ Å, $R_{Bi} = 1.45$ Å; $CN = 6$, $R_{Ti} = 0.605$ Å, $R_{Mg} = 0.72$ Å). However, it is clear that there is no dielectric relaxor behavior in 0.67BMT–0.33PT. This means that the static random electric fields or strain fields in these cases are so weak that PNRs cannot be generated or the generated PNRs are too large (static) in size [33,38,39]. Randall et al. [19] found that

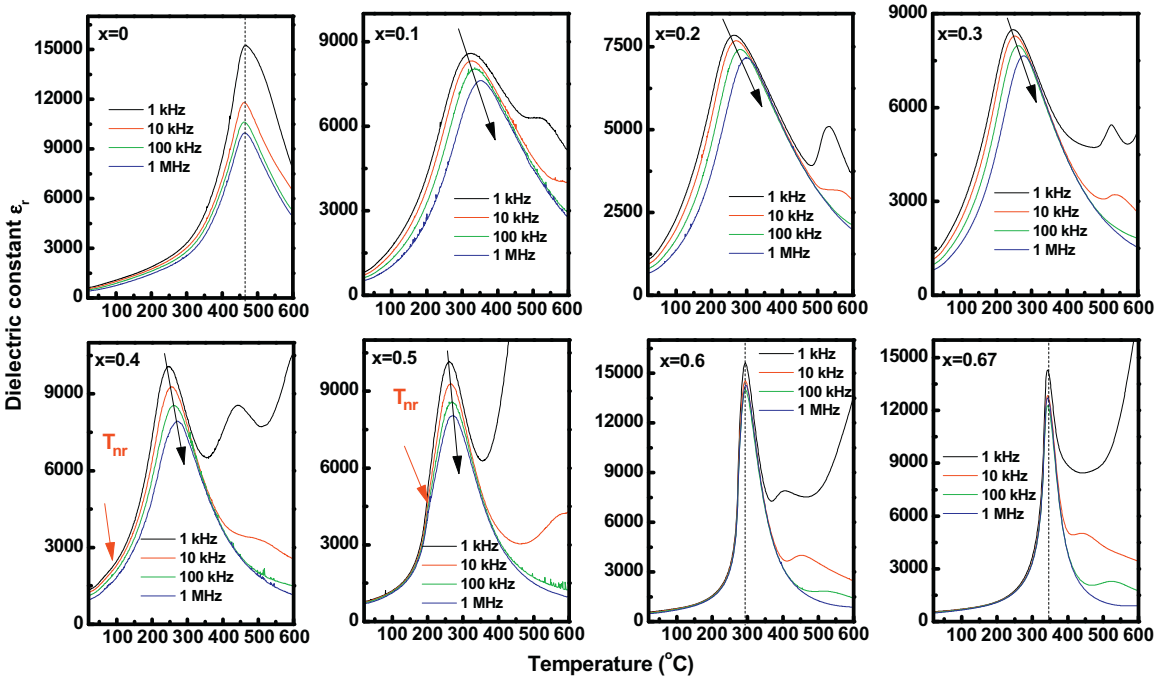

Fig. 3. Dielectric constants of BMT–xPZ–PT ceramics as a function of temperature and frequency.

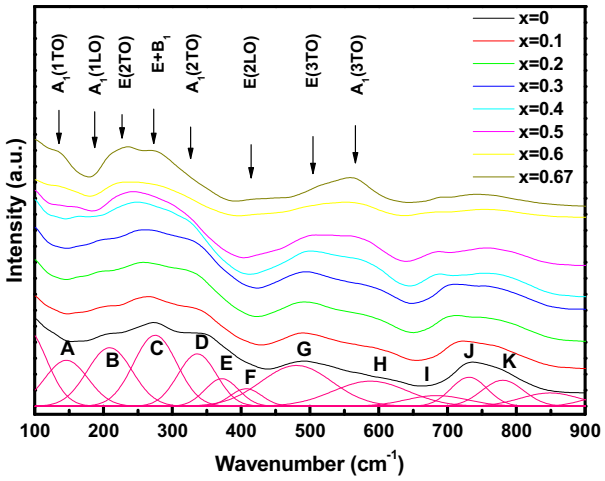

Fig. 4. Room-temperature Raman spectra of BMT–xPZ–PT as a function of the PZ content. The spectra were deconvoluted according to 11 Gaussian peak functions and the representative fitting is displayed only for the $x = 0$ sample.

the domain structure of rhombohedral BMT–PT ceramics consists of ~50 nm-sized polar microdomains, much larger than the PNRs in PMN relaxor. Therefore, the structural and/or chemical disorder might exist in BMT–PT but its domains are static and only can be switched under a sufficiently large electric field.

We can see that the above-mentioned dielectric behavior appears with the substitution of PZ for BMT. The role of Pb^{2+} can be excluded because similar dielectric behavior was never observed in BMT–PT solid solutions. However, a small shift of non-ferroactive Zr ions from the center of the oxygen octahedron can produce a small Zr polarization (i.e. the Zr–O polar dipoles), which tends to induce an additional dynamic random field in the initial static random field. This process can be accompanied by a decrease of the PNR size and an increase of the PNR dynamics. In addition, the small Zr polarization can be aligned under an electric field, which facilitates the switching of strong Ti–O polar dipoles by creating a favorable energetic situation. However, this phenomenon only exists in a perovskite with lone-pair A-site ions (e.g. PZT), because Zr ions usually lie in the center of the oxygen octahedron in a perovskite with ionic A-site ions (e.g. $BaTi_{1-x}Zr_{1-x}O_3$) [40,41].

3.4. Raman spectrum

It is known that any static and/or dynamic change in the local structure should induce a variation in the phonon behavior [42]. As a result, the analysis of the wave number, intensity and/or line width evolution of the Raman spectra for different samples was expected to give insight into the change in local structure evolution, as shown in Fig. 4. The broad Raman peaks mean that there exist obvious chemically ordered regions, and both the short- and long-range polar order. These broad Raman peaks correspond to three main regions and can be deconvoluted into different bands labeled as A-K from low to high frequencies. Each of the main regions corresponds to different types of lattice vibration. Only for the samples with high PZ contents ($x = 0.60$ and 0.67) can these peaks be assigned to the well-known Raman active modes similar to PZT with higher Zr contents [43]. In the low wave number region, e.g. at ~150 cm^{-1}, the modes are associated with the vibration of the perovskite A-site ions, such as Bi and Pb cations [42,44]. However, these vibrations were not considered in

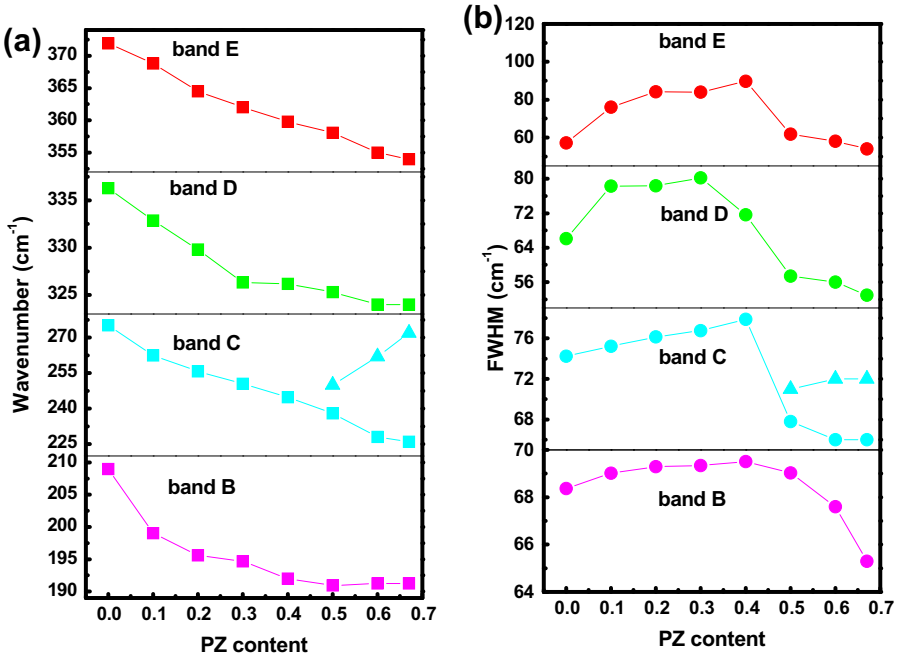

Fig. 5. Evolution of the wave number (a) and the FWHM (b) for Raman bands B-E in BMT–xPZ–PT ceramics.

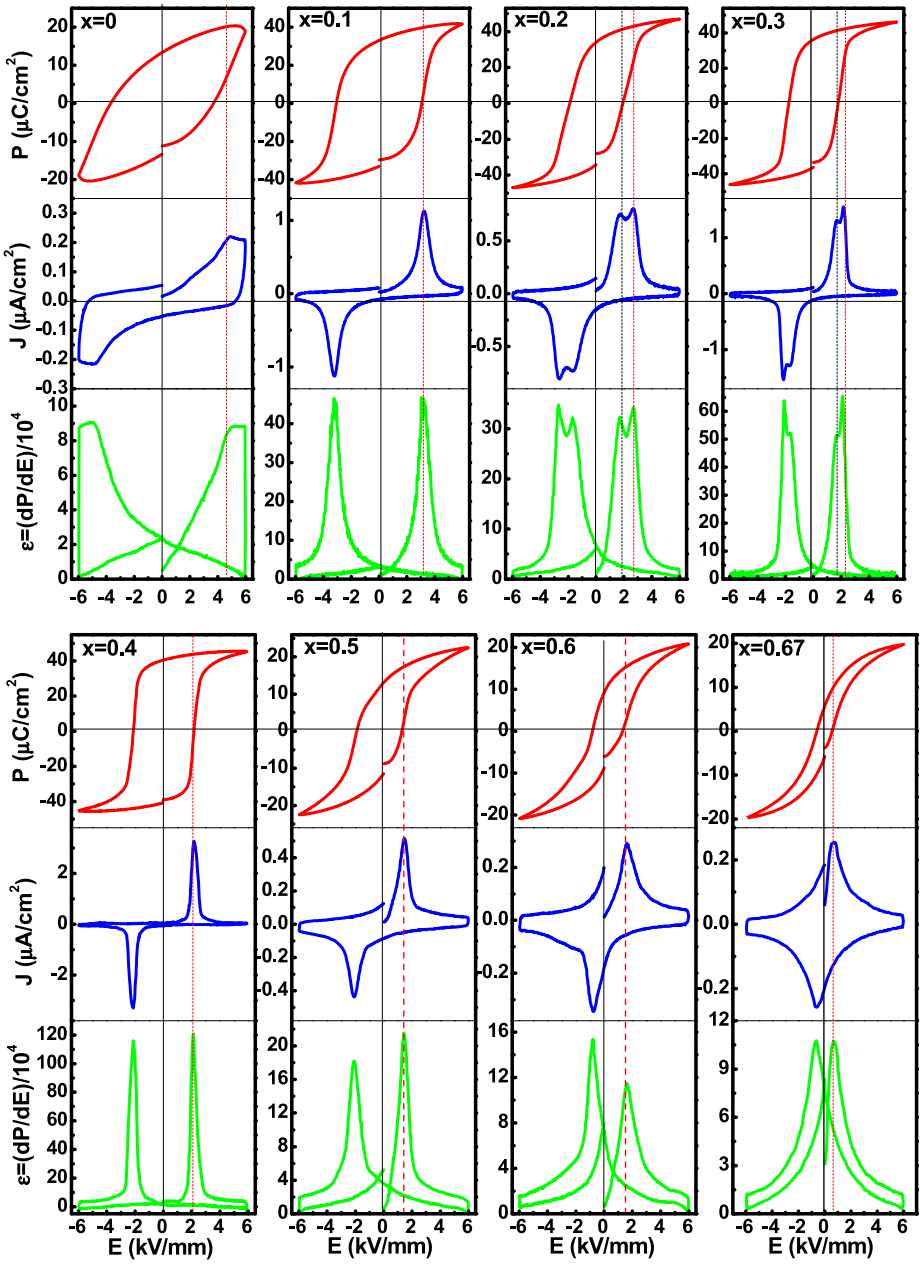

Fig. 6. The electric field induced polarization, polarization current density and dielectric response dP/dE of BMT–xPZ–PT ceramics as indicated.

the present analysis because the composition-induced relaxor behavior was rarely influenced by the change in the Bi/Pb ratio. The high-frequency bands above 450 cm^{-1} should be associated with the BO_6 vibrations, i.e. the breathing and stretching modes of the oxygen octahedra. By comparison, the 200–400 cm^{-1} wave number region characterized by four bands roughly at 200 cm^{-1} (band B), 260 cm^{-1} (band C), 330 cm^{-1} (band D) and 370 cm^{-1} (band E) in perovskite-structured ferroelectrics is of special interest because it is closely related with the B–O vibrations.

The evolution of the band position and full width at half maximum (FWHM) in this region was quantitatively extracted, as shown in Fig. 5. As we know, in the absence of any local structure transition, one would expect a steady phonon softening and an increase of FWHM with increasing the structure disorder and decreasing the unit cell polarity. As shown in Fig. 5, the B–O vibrations become softened gradually with increasing PZ content, which is due to a weakening of the bonding between the B-site cations and oxygen, particularly the strong Ti–O bonds. The weakening of the Ti–O bonds is compatible with the appearance of the macroscopic relaxor behavior since the variation of the Ti–O bonds is closely related with the dynamics of the PNRs [44]. In addition, it is found that the FWHMs of the B–O vibrations exhibit an obvious increase, leading to a strong composition disorder. However, both the wave numbers and the FWHMs of the B–

O vibrations show drastic changes from $x = 0.4$ to $x = 0.5$, i.e. the splitting of the band C and the drastic decrease of the FWHMs. This abrupt change was believed to correspond to the relaxor–normal ferroelectric transition as evidenced in Fig. 3.

4. Discussion

From the above S–E curves, ε–T curves and Raman spectrum, one can conclude that a giant electrostrain accompanies the appearance of a relaxor behavior in the BMT–PZ–PT ternary system. It is generally believed that PNRs play an important role in the relaxor behavior. The strong interaction between the PNRs in relaxors consequently tends to bring about the large electrostriction and piezoelectricity [45,46]. However, the electrostrictive strain is usually proportional to the square of the polarization and shows negligible S_{neg}. In the present study, the relaxor state induced by the Zr substitution should be a nonergodic relaxor state instead of a dipole glass state because we have observed all essential features of nonergodic relaxor behavior rather than the dipole glass freezing in the BMT–xPZ–PT relaxors [33,47]. Fig. 6 demonstrates some typical results of the electric-field-induced polarization, polarization current density J (dP/dt) and dielectric response dP/dE for different compositions. It can be seen that all compositions show a normal polarization switching behavior as observed in PMN in a low temperature range [47]. In addition, double peaks in J curves or dP/dE curves can be obviously observed in the sample with $x = 0.2$ and 0.3, suggesting that the polarization switching process under bipolar cycles consists of two steps. One is the polarization reorientation of the PNRs and the other is the coalescence of PNRs into the macroscopic ferroelectric domains, leading to larger remanent polarization values. With increasing PZ content, these two steps merge into a single one gradually and the activation field required for the polarization reorientation decreases monotonously. It is interesting to note that the enhancement of the S_E (or S_{pos}) value should be associated with the reduction of the S_{neg} value in the composition range of $x = 0$–0.4. This phenomenon was also found in $(Bi_{0.5}Na_{0.5})TiO_3$-based materials [48]. The $x = 0.2$ BMT–PZ–PT sample with the largest S_E (or S_{pos}) value exhibits a typical butterfly-like strain loop and a saturated polarization hysteresis loop. However, for $(Bi_{0.5}Na_{0.5})TiO_3$-based materials, the composition with the largest S_E exhibits antiferroelectric-like loops. Its strain value can be well linearly related to the square of the polarization as follows:

$$S = Q_{ij}P^2 \quad (1)$$

although strain loops are obviously hysteretic. This is quite different from the S–P^2 curves observed in BMT–xPZ–PT ternary system, as shown in Fig. 7. On the one hand, the reorientation of the PNRs in BMT–PT binary system becomes much easier owing to the substitution of Zr^{4+}. On the other hand, the transformation between the PNRs and the ferroelectric states can be easily driven by external electric fields because both states own the same crystal symmetry and comparable free energies. These two effects would generate an enhanced switching of the PNRs, thus inducing giant electrostrains in BMT–xPZ–PT samples, particularly for the $x = 0.2$ composition.

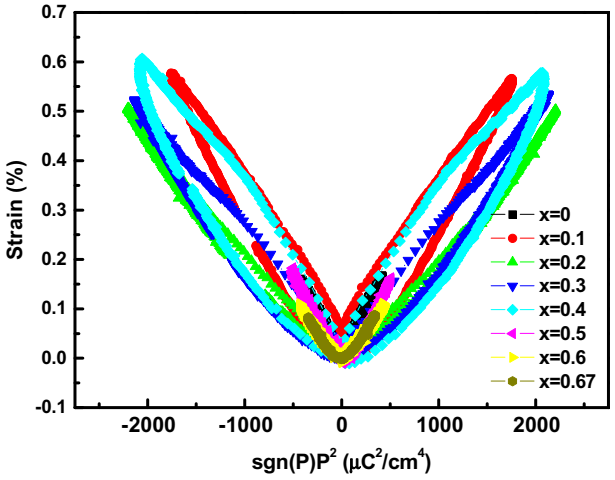

Fig. 7. Strains as a function of P^2 for BMT–xPZ–PT ceramics at room temperature.

5. Conclusions

The composition-induced realxor behavior and its correlation with the giant electrostrains in BMT–xPZ–PT ceramics were investigated. The significantly enhanced electrostrains as large as 0.39% were generated in BMT–xPZ–PT ternary solid solutions. The generation of such giant strains was believed to be closely associated with the evolution of a weak relaxor behavior from diffuse-type BMT–PT binary ferroelectrics, during which the domain switching can be actively facilitated owing to a change in the dynamics of the polar nanoregions from a static state to a dynamic state. Moreover, it could be also ascribed to a ferroelectric nature of the evolved relaxors in PZ substituted BMT–PT ceramics, instead of a dipole glass freezing state. These judgements were reasonably supported by a couple of measurements including strains vs. electric field, Raman scattering, dielectric spectroscopy and the time- and electric-field-dependent polarization. The present study can provide a general approach towards an appropriate compositional design for large electrostrains in BMT-based and related systems.

Acknowledgements

This work was financially supported by the National Natural Science Foundation of China (51272060) and the Natural Science Foundation of Anhui province (1108085J14).

References

[1] Park SE, Shrout TR. J Appl Phys 1997;82:804.
[2] Bhattacharya K, Ravichandran G. Acta Mater 2003;51:5941.
[3] Hoffmann MJ, Kungl H. Curr Opin Solid St M 2004;8:51.
[4] Zhang ST, Kounga AB, Jo W, Jamin C, Seifert K, Granzow T, et al. Adv Mater 2009;21:4716.
[5] Shebanov L, Kusnetsov M, Sternberg A. J Appl Phys 1994;76:4301.
[6] Park SE, Pan MJ, Markowski K, Yoshikawa S, Cross LE. J Appl Phys 1997;82:1798.
[7] Durbin MK, Jacobs EW, Hicks JC, Park SE. Appl Phys Lett 1999;74:2848.
[8] Fu HX, Cohen RE. Nature 2004;403:281.
[9] Guo R, Cross LE, Park SE, Noheda B, Cox DE, Shirane G. Phys Rev Lett 2000;84:5423.
[10] Noheda B, Cox DE, Shirane G, Park SE, Cross LE, Zhong Z. Phys Rev Lett 2001;86:3891.
[11] Kutnjak Z, Petzelt J, Blinc R. Nature 2006;44:956.
[12] Kornev IA, Bellaiche L, Janolin PE, Dkhil B, Suard E. Phys Rev Lett 2006;97:157601.
[13] Davis M, Damjanovic D, Setter N. Phys Rev B 2006;73:014115.
[14] Ge WW, Ren Y, Zhang JL, Devreugd CP, Li JF, Viehland D. J Appl Phys 2011;111:103503.
[15] Fu J, Zuo RZ, Wu SC, Jiang JZ, Li L, Yang TY, et al. Appl Phys Lett 2012;100:122902.
[16] Zuo RZ, Fu J, Yin GZ, Li XL, Jiang JZ. Appl Phys Lett 2012;101:092906.
[17] Li F, Zhang SJ, Xu Z, Wei XY, Luo J, Shrout TR. Appl Phys Lett 2010;96:192903.
[18] Li JY, Rogan RC, Üstündag E, Bhattacharya K. Nat Mater 2005;4:776.
[19] Randall CA, Eitel R, Jones B, Shrout TR, Woodward DI, Reaney IM. J Appl Phys 2004;95:3633.
[20] Moure A, Algueró M, Pardo L, Ringgaard E, Pedersen AF. J Eur Ceram Soc 2007;27:237.
[21] Hu PH, Chen J, Sun XY, Deng JX, Chen X, Yu RB, et al. J Mater Chem 2009;19:1648.
[22] Zhang Q, Li ZR, Li F, Xu Z, Yao X. J Am Ceram Soc 2010;93:3330.
[23] Sebastian T, Sterianou I, Reaney IM, Leist T, Jo W, Rödel J. J Electroceram 2012;28:95.
[24] Dwivedi A, Qu WG, Randall CA. J Am Ceram Soc 2011;94:4371.
[25] Dwivedi A, Randall CA, Rossetti GA. Mater Lett 2011;65:3034.
[26] Jaffe B, Cook WR, Jaffe H. Piezoelectric ceramics. London: Academic Press; 1971.
[27] Shannon RD. Acta Cryst A 1976;32:751.
[28] Kungl H, Theissmann R, Knapp M, Baehtz C, Fuess H, Wagner S, et al. Acta Mater 2007;55:1849.
[29] Shvartsman VV, Kleemann W, Dec J, Xu ZK, Lu SG. J Appl Phys 2006;99:124111.
[30] Dwivedi A, Randall CA. J Appl Phys 2011;109:074102.
[31] Xie L, Li YL, Yu R, Cheng ZY, Wei XY, Yao X, et al. Phys Rev B 2012;85:014118.
[32] Bobnar V, Kutnajak Z, Pirc R, Blinc R, Levstik A. Phys Rev Lett 2000;84:5892.
[33] Bokov AA, Ye ZG. J Mater Sci 2006;41:31.
[34] Chu F, Reaney IM, Setter N. J Appl Phys 1995;77:1671.
[35] Dai XH, Xu Z, Viehland D. J Appl Phys 1996;79:1021.
[36] Deng GC, Ding AL, Li GR, Zheng XS, Cheng WX, Qiu PS, et al. J Appl Phys 2005;98:094103.
[37] Suewattana M, Singh DJ, Limpijumnong S. Phys Rev B 2012;86:064105.
[38] Shvartsman VV, Lupascu DC. J Am Ceram Soc 2012;95:1.
[39] Singh A, Moriyoshi C, Kuroiwa Y, Pandey D. Phys Rev B 2012;85:064116.
[40] Laulhé C, Hippert F, Kreisel J, Maglione M, Simon A, Hazemann JL, et al. Phys Rev B 2006;74:014106.
[41] Al-Zein A, Fraysse G, Rouquette J, Papet Ph, Haines J, Hehlen B, et al. Phys Rev B 2010;81:174110.
[42] Haumont R, Gemeiner P, Dkhil B, Kiat JM, Bulou A. Phys Rev B 2006;73:104106.
[43] Lima KCV, Filho AGS, Ayala AP, Filho JM, Freire PTC, Melo FEA, et al. Phys Rev B 2001;63:184105.
[44] Schütz D, Deluca M, Krauss W, Feteira A, Jackson T, Reichmann K. Adv Funct Mater 2012;22:2285.
[45] Pirc R, Blinc R, Vikhnin VS. Phys Rev B 2004;69:212105.
[46] Xu GY, Wen JS, Stock C, Gehring PM. Nat Mater 2008;7:562.
[47] Fu DS, Taniguchi H, Itoh M, Koshihara S, Yamamoto N, Mori S. Phys Rev Lett 2009;103:207601.
[48] Guo YP, Liu Y, Withers RL, Brink F, Chen H. Chem Mater 2011;23:219.